

Shear Particle Acceleration in Structured Gamma-Ray Burst Jets: I. Physical Origin of the Band Function and Application to GRBs 090926A, 131108A, and 160509A

ZI-QI WANG,¹ XIAO-LI HUANG^{*,2,1} AND EN-WEI LIANG^{*1}

¹Guangxi Key Laboratory for Relativistic Astrophysics, School of Physical Science and Technology, Guangxi University, Nanning 530004, People's Republic of China

²School of Physics and Electronic Science, Guizhou Normal University, Guiyang 550025, People's Republic of China

ABSTRACT

The radiation physics of gamma-ray bursts (GRBs) remains an open question. Based on the simulation analysis and recent observations, it was proposed that GRB jets are composed of a narrow ultra-relativistic core surrounded by a wide sub-relativistic cocoon. We show that emission from the synchrotron radiations and the synchrotron self-Compton (SSC) process of shear-accelerated electrons in the mixed jet-cocoon (MJC) region and internal-shock-accelerated electrons in the jet core is potentially explained the spectral characteristics of the prompt gamma-rays. Assuming an exponential-decay velocity profile, the shear flow in the MJC region can accelerate electrons up to $\gamma_{e,\max} \sim 10^4$ for injected electrons with $\gamma_{e,\text{inject}} = 3 \times 10^2$, if its magnetic field strength (B_{cn}) is 100 G and its inner-edge velocity ($\beta_{\text{cn},0}$) is 0.9c. The cooling of these electrons is dominated by the SSC process, and the emission flux peaks at the keV band. In addition, the energy flux of synchrotron radiations of internal-shock-accelerated electrons ($\gamma_e = 10^4 \sim 10^5$) peaks at around the keV–MeV band, assuming a bulk Lorentz factor of 300, a magnetic field strength of $\sim 10^6$ G for the jet core. Adding the flux from both the jet core and the MJC region, the total spectral energy distribution (SED) illustrates similar characteristics as the broadband observations of GRBs. The bimodal and Band-Cut spectra observed in GRBs 090926A, 131108A, and 160509A can be well fit with our model. The derived B_{cn} varies from 54 G to 450 G and $\beta_{\text{cn},0} = 0.83 \sim 0.91c$.

Keywords: Gamma-ray bursts (629); Non-thermal radiation sources (1119)

1. INTRODUCTION

Gamma-ray bursts (GRBs) are extreme electromagnetic events in the universe. Extensive observations with gamma-ray missions have accumulated a large sample of GRB spectra in the keV–MeV–GeV bands. Specifically, the GRB spectrum in the keV–MeV band observed with the Burst And Transient Source Experiment (BATSE, 20–1000 keV) on-board the Compton Gamma-Ray Observatory (CGRO) mission is typically fitted with a smooth broken power-law function, known as the Band function (Band et al. 1993; Kaneko et al. 2006). This characteristic is also confirmed with observations of the Gamma-Ray Burst Monitor (GBM, 15–1000 keV) on-board the *Fermi* Gamma-ray Space Telescope (Zhang et al. 2011; Poolakkil et al. 2021). Furthermore, the joint spectra of some GRBs observed with both the GBM and the Large Area Telescope (LAT) on-board the *Fermi* in the 8 keV–300 GeV range exhibit either a bimodal structure (such as GRB 090926A; Ackermann et al. 2011; Yassine et al. 2017) or a Band function with cut-off (the so-called Band-Cut function; Ackermann et al. 2013; Tang et al. 2017). It is indicated that the spectra of generic GRBs in the keV–GeV band maybe embed an extra component beneath the Band function (Zhang et al. 2011).

It is suggested that GRBs originate from ultra-relativistic jets powered by collapses of massive stars or mergers of compact object (Narayan et al. 1992; Woosley 1993; Mészáros 2002; Piran 2004; Kumar & Zhang 2015). Within the framework of the standard jet model, a photosphere stage and an internal dissipation stage (internal shocks, internal magnetic processes, etc.) are expected (Paczynski 1986; Rees & Meszaros 1994; Daigne & Mochkovitch 1998;

Mészáros & Rees 2000; Lyutikov & Blandford 2003; Zhang & Yan 2011). Consequently, the predicted prompt emission spectrum may consist of a thermal component from the photosphere emission and a non-thermal component from the synchrotron (Syn) and/or the Inverse Compton (IC) emission of the accelerated electrons (Goodman 1986; Rees & Meszaros 1994; Pilla & Loeb 1998). Furthermore, the propagation of a relativistic jet through the surrounding medium drives a bow shock, forming a cocoon of shocked material that deposits significant energy (Aloy et al. 2000; Zhang et al. 2003; Bromberg et al. 2011; Matsumoto & Masada 2019). When the jet breakout, the cocoon material erupts and disperses radially and axially, resulting in the formation of a jet-cocoon structure (Ramirez-Ruiz et al. 2002; Morsony et al. 2007). Such a jet-cocoon structure has been the focus of intensive investigations (Lazzati & Begelman 2005; Pe’er et al. 2006; Nakar & Piran 2017; Lazzati & Perna 2019). GRBs 170817A and 221009A are two representative cases for revealing the GRB ejecta structure. The observed short GRB 170817A, associated with the binary neutron star merger gravitational wave (GW) signal GW170817 (Abbott et al. 2017a,b), has been suggested to be attributable to off-axis observations of a structured ejecta with a large viewing angle (Biehl et al. 2018; Mooley et al. 2018; Gottlieb et al. 2018; Fraija et al. 2019). On the other hand, the broadband afterglow lightcurves of long GRB 221009A are fitted by considering a core-wing configuration (O’Connor et al. 2023; Sato et al. 2023; Gill & Granot 2023; Ren et al. 2024).

Relativistic hydrodynamic and magnetohydrodynamic simulations reveal a radial velocity distribution within the jet-cocoon outflow, that is known as shear flow (Aloy et al. 2000; Tchekhovskoy et al. 2008; Mizuta & Ioka 2013; Gottlieb & Globus 2021). Particles could be accelerated within the shear flow (Berezhko & Krymskii 1981; Webb 1989; Rieger & Duffy 2004; Webb et al. 2018). The shear-accelerated electrons may be expected as a potential contributor to the prompt emission of GRBs. As a result, the prompt gamma-ray spectrum may be shaped by two distinct electron populations: one accelerated by internal shocks via the Fermi acceleration mechanism within the jet, and the other by the shear acceleration mechanism within the mixed jet-cocoon (MJC) region. In this paper, we investigate a comparative analysis of the GRB radiation in the framework of synchrotron and SSC emissions of electrons accelerated in the jet core and the MJC region. We present our model in Sec. 2 and apply this model to fit the spectra of GRBs 090926A, 131108A, and 160509A in Sec. 3. The spectra of these GRBs display a bimodal feature or a deviation from the standard Band function profile. The summary and discussion are presented in Sec. 4. Throughout this paper, we employ a Hubble constant of $H_0 = 71 \text{ kms}^{-1} \text{ Mpc}^{-1}$, and the cosmological parameters of $\Omega_M = 0.27$ and $\Omega_\Lambda = 0.73$.

2. MODEL

2.1. Jet-Cocoon Structure

Motivated by the results of numerical simulations and theoretical calculations, we conceptualize the GRB ejecta as a jet-cocoon structure, as illustrated in Figure 1. This structure consists of three distinct regions: an ultra-relativistic narrow jet core region with an uniform velocity profile ($r < r_0$), a sub-relativistic mixed jet-cocoon region with decreasing velocity as a function of radial radius ($r_0 < r < r_2$), and an outer cocoon region with a uniform velocity profile ($r > r_2$). Moreover, particle-in-cell (PIC) simulations have demonstrated significant particle acceleration at the shear boundary layer (SBL) (Alves et al. 2014). We also illustrate the SBL as a thin layer at $r_0 \lesssim r \lesssim r_1$. Hereinafter, variables with the subscripts “jet” and “cn” refer to the jet and cocoon regions, respectively.

We set the distance of the emitting regions of both the jet and MJC region from the central engine as R (Ramirez-Ruiz et al. 2002; Zhang & Yan 2011; Pe’er 2015). In the framework of jet-cocoon structure, we postulate that the GRB ejecta during the prompt emission phase remains in a steady-state scenario, with no significant density variation and lateral (radial) expansion. We consider that the velocity \mathbf{u} of MJC region is along the direction of the jet axis (i.e. $\mathbf{u} = u_{\text{cn}}(r)\mathbf{e}_z$), and the velocity profile is modeled as an exponential-decay function

$$u_{\text{cn}}(r) = \beta_{\text{cn},0} e^{-k}, \quad k = \frac{r \ln(\beta_{\text{cn},0}/\beta_{\text{cn},2})}{r_2}, \quad (1)$$

where r is the radial distance from the jet axis, u_{cn} is the outflow velocity in units of the light speed c , $\beta_{\text{cn},0}$ and $\beta_{\text{cn},2}$ are the fluid velocities at r_0 and r_2 , respectively. Theoretically, the velocity of the outer cocoon ejecta should not exceed the local sound speed. In this work, we constrain the boundary velocity to $\beta_{\text{cn},2} < 1/\sqrt{3}$ (Ramirez-Ruiz et al. 2002; Mizuta et al. 2010). We assume an uniform magnetic field strength within the jet core and the MJC region.

2.2. Particle Acceleration in the MJC region

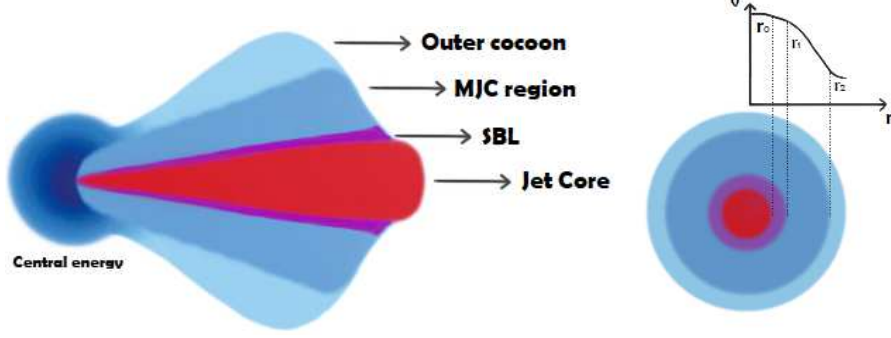


Figure 1. The schematic diagram of the Jet-Cocoon structure.

Particles could be accelerated through the shear acceleration mechanism in the MJC region. This process involves the coupling of the energetic particles and the shear force in the outflow due to cosmic-ray viscosity, as well as the scattering process arising from magnetic field irregularities embedded in the background outflow (Berezhko & Krymskii 1981; Webb 1989; Rieger & Mannheim 2002; Rieger & Duffy 2004; Webb et al. 2018).

As mentioned above, PIC simulations show significant particle acceleration at the SBL, attributed to the combined effects of instabilities and electromagnetic fields (Alves et al. 2012; Liang et al. 2017). This also leads to notable particle accumulation within the SBL. The SBL sustains a prolonged particle acceleration process and efficiently energizes the majority of particles. For leptons, this mechanism maybe achieve energies characterized by $\gamma_{\text{eff}} \sim \Gamma_{\text{jet}}$, proceeding in a strongly an-isotropic manner (Liang et al. 2017). Therefore, we designate the SBL as an electron injection layer of the MJC region and assume the injected electrons are a mono-energetic population with $\gamma_{e,\text{inject}} = \gamma_{\text{eff}}$.

The injected electrons are further accelerated in the MJC region. We focus on the strong scattering limit case, where collisions are sufficiently effective to restore isotropy (Rieger & Duffy 2005). Based on the strong particle scattering assumption, Webb et al. (2018) provides a steady-state solution for particle acceleration in the relativistic shear flow within the isotropic diffusion model. When the scattering wave frame is taken to coincide with the comoving fluid frame, the transport equation for the isotropic shear-accelerated particles distribution function $f_0(x^\alpha, p)$ ($x^\alpha = (ct, x, y, z)$) in momentum space can be expressed as (Skilling 1975; Webb 1989; Webb et al. 2018)

$$\begin{aligned} & \nabla_\alpha \left[cu^\alpha f_0 - \kappa (\eta^{\alpha\beta} + u^\alpha u^\beta) \left(\frac{\partial f_0}{\partial x^\beta} - \dot{u}_\beta \frac{(p^0)^2}{p} \frac{\partial f_0}{\partial p} \right) \right] \\ & + \frac{1}{p^2} \frac{\partial}{\partial p} \left[-\frac{p^3}{3} cu_{;\beta}^\beta f_0 + p^3 \left(\frac{p^0}{p} \right)^2 \right. \\ & \left. \times \kappa \dot{u}^\beta \left(\frac{\partial f_0}{\partial x^\beta} - \dot{u}_\beta \frac{(p^0)^2}{p} \frac{\partial f_0}{\partial p} \right) - \Lambda \tau p^4 \frac{\partial f_0}{\partial p} \right] = Q, \end{aligned} \quad (2)$$

where $\eta^{\alpha\beta}$ is the Minkowski metric (scripts $\alpha, \beta = 0, 1, 2, 3$), u^α denotes the fluid velocity four-vector, and \dot{u} represents the acceleration vector of the fluid, $u_{;\beta}^\beta$ represents the covariant derivative. p is the comoving particle momentum, $p^0 = E/c$ is the zeroth component of the particle momentum four-vector in the fluid frame. τ is the scattering or collision timescale. κ is the particle diffusion coefficient ($\kappa = v^2\tau/3$, where v is the particle speed in the comoving frame). Q represents particle source, and Λ quantifies the viscous energization coefficient. Under the strong scattering limit, Λ is given by

$$\Lambda = \frac{c^2}{30} \sigma_{\alpha\beta} \sigma^{\alpha\beta}, \quad (3)$$

where $\sigma_{\alpha\beta}$ is the shear tensor of the background flow (Webb 1989; Webb et al. 2018).

We consider particles to be bounded within the MJC region ($r_0 < r < r_2$) where the outflow is treated as steady-state and incompressible. Particles are injected into the region at $r = r_1$ ($r_1 \gtrsim r_0$) with the momentum $p_0 \sim \gamma_{e,\text{inject}}/m_e c$, and escape from the acceleration region at $r = r_2$. The particle source term Q is given by

$$Q = \frac{1}{2\pi r_1} \frac{N_0}{4\pi p_0^2} \delta(p - p_0) \delta(r - r_1), \quad (4)$$

where N_0 is the initial distribution of injected electrons. In accordance with the strong scattering limit, we assume a relatively weak average magnetic field and strong turbulence within the MJC region (Spruit et al. 2001; Rieger & Duffy 2005; Zrake & MacFadyen 2012).

Then the covariant derivative $u_{;\beta}^\beta$ can be specified as $u_{;\beta}^\beta = 0$, and the viscous energization coefficient Λ has the form

$$\Lambda = \frac{c^2}{15} \Gamma_{\text{cn}}^4 \left(\frac{du_{\text{cn}}}{dr} \right)^2. \quad (5)$$

Accordingly, in the steady-state relativistic MJC region within the GRB environment, the transport equation (Eq. 2) for the distribution function of shear-accelerated electrons can be recast as

$$-\frac{1}{r} \frac{\partial}{\partial r} \left(\kappa r \frac{\partial f_0}{\partial r} \right) - \frac{c^2}{15} \frac{\Gamma_{\text{cn}}^4}{p^2} \left(\frac{du_{\text{cn}}}{dr} \right)^2 \frac{\partial}{\partial p} \left(p^4 \tau \frac{\partial f_0}{\partial p} \right) = \frac{N_0 \delta(p - p_0) \delta(r - r_1)}{8\pi^2 p_0^2 r_1}. \quad (6)$$

The analytical solution of Eq. 6 for the shear-accelerated electron distribution function f_0 can be formulated as (Webb et al. 2018)

$$f_0 = \frac{15}{8\pi^2 (\xi_0 - \xi_2) \left| \frac{d\xi}{dr} \right|_{r_1}} \left(\frac{N_0}{p_0^3 c^2 \tau_0} \right) \exp \left[-\frac{(3 + \alpha) T}{2} \right] \\ \times \sum_{n=0}^{\infty} \frac{1}{y_n} \sin \left[\left(n + \frac{1}{2} \right) \pi w_1 \right] \sin \left[\left(n + \frac{1}{2} \right) \pi w \right] \exp(-y_n |T|), \quad (7)$$

in which

$$\xi(r) = \frac{1}{2} \ln \left(\frac{1 + u_{\text{cn}}}{1 - u_{\text{cn}}} \right), \quad w \equiv \frac{\xi - \xi_2}{\xi_0 - \xi_2}, \quad T = \ln \left(\frac{p}{p_0} \right) \quad (8)$$

$$y_n = \left[\frac{5\pi^2 (2n + 1)^2}{4 (\xi_0 - \xi_2)^2} + \frac{(3 + \alpha)^2}{4} \right]^{1/2}, \quad n = 0, 1, 2, \dots, \quad (9)$$

where the subscripts 0, 1, and 2 represent the physical quantities at $r = r_0$, $r = r_1$, and $r = r_2$, respectively. τ_0 is the initial scattering timescale and $\alpha = 2 - q$ is a constant that determines the momentum dependence of the mean scattering time τ . q is the spectral index of the turbulence model. Employing the Kolmogorov turbulence model, we ascertain the wave number spectral index as $q = 5/3$, corresponding to $\alpha = 1/3$ (Kolmogorov 1941).

In the frame of the quasi-linear theory, the scattering time (τ) can be consistent with the mean free path formula (λ) (Liu et al. 2017; Webb et al. 2018). τ and λ are given by

$$\tau(r, p) = \tau_0 \left(\frac{p}{p_0} \right)^\alpha \frac{r_1 \xi'(r_1)}{r \xi'(r)}, \quad \lambda = \frac{r_g^{2-q} \ell_b^{q-1}}{c \chi} N(q), \quad (10)$$

where $N(q) = 3/[(2 - q)(4 - q)]$, $r_g = pc/(eB_{\text{cn}})$ is the gyroradius of particle, $\ell_b = 1/k_b$ corresponds roughly to the correlation length of the turbulence, and

$$\chi = \left(\frac{\delta B_{\text{cn}}}{B_{\text{cn}}} \right)^2 \frac{1}{\Phi(k_b, k_d)}, \quad \Phi(k_b, k_d) = 1 + \frac{1 - (k_b/k_d)^{1-q}}{q - 1}, \quad (11)$$

in which δB_{cn} is the magnetic field fluctuation perpendicular to the magnetic field B_{cn} ($\delta B_{\text{cn}} \ll B_{\text{cn}}$; Zank et al. 2004; Liu et al. 2017), k_b and k_d are the range of resonant wave number for interactions. In our analysis, the parameters k_b and k_d ideally keep as $k_b = 10^{-13}$ cm and $k_d = 10^{-2}$ cm, respectively (Biskamp 2003; Webb et al. 2018). With $\tau = \lambda$, τ_0 can be inferred as

$$\tau_0 = \left(\frac{\ell_b}{c} \right) \frac{N(2 - q)}{\chi(r_1)} \left(\frac{p_0 c}{\ell_b e B_{\text{cn}}} \right)^\alpha. \quad (12)$$

We calculate shear-accelerated particle distributions within the MJC region. The parameters of the MJC region are set as follows: the distance to the central engine $R = 10^{15}$ cm, the full opening angles $\theta_{\text{cn}} = 0.7$ rad, the magnetic field strength $B_{\text{cn}} = 100$ G (Spruit et al. 2001; Pe'er et al. 2006), and $\gamma_{e,\text{inject}} = 300$. Figure 2 illustrates the velocity profiles

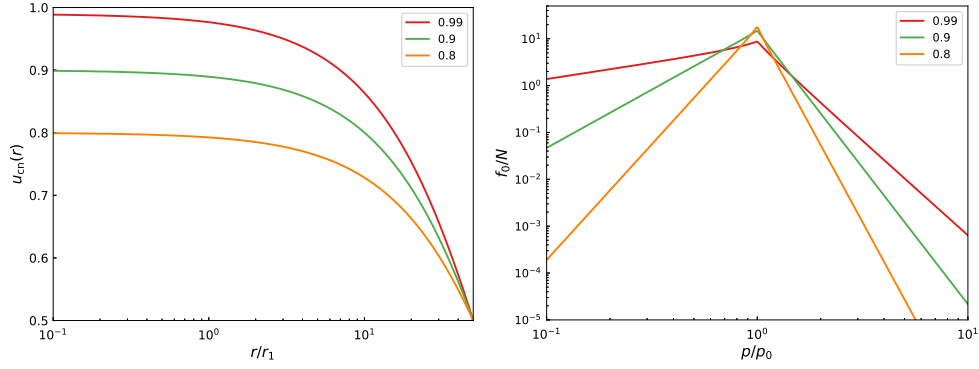


Figure 2. Left panel– Velocity profiles of the MJC region as an exponential-decay function of radius, with initial velocities of $\beta_{\text{cn},0} = 0.99, 0.9, 0.8$. Right panel– Distributions of shear-accelerated electrons for exponential-decay velocity profiles as shown in the left panel, where $N = N_0 / (p_0^3 c^2 \tau_0 r_1 | \frac{d\xi}{dr} |_{r_1})$.

for various $\beta_{\text{cn},0}$ values and the corresponding electron distributions accelerated via the shear acceleration mechanism. One can find that the particle distribution is broader for larger $\beta_{\text{cn},0}$. At the high momentum band ($p > p_0$), the shear-accelerated particle distribution exhibits a power-law decay behavior, which is characterized by $f_0 \propto p^{-\mu_\infty}$. Based on Eq. (7), the spectral index μ_∞ is given by (Webb et al. 2018)

$$\mu_\infty = \left(\frac{5\pi^2}{4(\xi_0 - \xi_2)^2} + \frac{(3 + \alpha)^2}{4} \right)^{1/2} + \frac{(3 + \alpha)}{2}. \quad (13)$$

At the low energy band ($p < p_0$), the spectrum initially presents as an inverse power-law behavior, described by $f_0 \propto p^{-\mu_0}$ when $p \rightarrow 0$. The power law index μ_0 is defined as

$$\mu_0 = \left(\frac{5\pi^2}{4(\xi_0 - \xi_2)^2} + \frac{(3 + \alpha)^2}{4} \right)^{1/2} - \frac{(3 + \alpha)}{2} = \mu_\infty - (3 + \alpha). \quad (14)$$

The particle distribution resulting from shear acceleration is dramatically different from the typical first-order Fermi acceleration ($f_{\text{st}} \propto p^{-q_{\text{st}}}$) and second-order Fermi acceleration ($f_{\text{nd}} \propto p^{-2} e^{3-q_{\text{nd}}}$) (Ellison et al. 1990; Keshet & Waxman 2005; Murase et al. 2012).

The maximum shear-accelerated electron Lorentz factor $\gamma_{M,\text{cn}}$ is restricted by $t_{\text{acc},\text{cn}} = t_{\text{rad},\text{cn}}$, where $t_{\text{acc},\text{cn}}$ is the shear acceleration timescale and $t_{\text{rad},\text{cn}}$ is the cooling timescale via the synchrotron radiation and the synchrotron self-Compton (SSC) process. The $t_{\text{acc},\text{cn}}$ is estimated as (Webb et al. 2018)

$$t_{\text{acc},\text{cn}} = \frac{p}{\langle \Delta p / \Delta t \rangle} = \frac{15}{(4 + \alpha) \Gamma_{\text{cn}}^4 (du_{\text{cn}}(r)/dr)^2 \tau}, \quad (15)$$

where Γ_{cn} is the Lorentz factor of the cocoon region, and τ is given by Eq. 10. The $t_{\text{rad},\text{cn}}$ value is calculated with (Nakar et al. 2009)

$$t_{\text{rad},\text{cn}} = t_{\text{Syn}_{\text{cn}}} + t_{\text{SSC}_{\text{cn}}} = \frac{6\pi m_e c}{\gamma_{e,\text{cn}} \sigma_T B_{\text{cn}}^2 (1 + Y_{\text{cn}})}, \quad (16)$$

where Y_{cn} is the Compton parameter, defined as the ratio of the SSC_{cn} power to the Syn_{cn} power. The radial scale of the MJC region is estimated as $r_{\text{cn}} \simeq \theta_{\text{cn}}/2 \times R = 3.5 \times 10^{14}$ cm. Taking $\beta_{\text{cn},0} = 0.9$, $B_{\text{cn}} = 100$ G, $\gamma_{e,\text{inject}} = 3 \times 10^2$, we have $\gamma_{M,\text{cn}} \sim 10^4$. These electrons should also be confined in the acceleration region. This requires that the gyroradius (r_g) of the electron is smaller than the maximum wavelength (ℓ_b) for particle scattering. Considering that particle scattering is primarily influenced by turbulence within the inertial range, we have $\ell_b = \eta r_{\text{cn}}$, where $\eta \lesssim 1$ (Liu et al. 2017; Webb et al. 2018). Based on above parameters, the r_g of electrons with $\gamma_{e,\text{cn}} = 10^4$ is $\sim 10^{13}$ cm. Therefore, we have $\ell_b > r_g$. In addition, we also estimate the dynamic timescale of the injected electrons as $t_{\text{dyn}} \sim r_{\text{cn}}/c\beta_{\text{cn},0} \sim 10^4$ s. It is evident that t_{dyn} is much larger than $t_{\text{acc},\text{cn}}$. These results suggest that the shear acceleration process operates efficiently within the MJC region.

2.3. Radiation Mechanism and Spectral Energy Distribution

The electrons accelerated via the shear acceleration mechanism within the MJC region and through internal shocks in the jet core region are cooled by both the Syn radiation and the SSC process. The parameters of the MJC region and the corresponding shear-accelerated electron distributions are taken as discussed above. We assume the parameters of the jet core as follows: the distance to the central engine $R = 10^{15}$ cm, bulk Lorentz factor $\Gamma_{\text{jet}} = 300$, full opening angle $\theta_{\text{jet}} = 0.07$ rad, and the magnetic field strength $B_{\text{jet}} = 10^6$ G (Bustamante et al. 2017). The shock-accelerated electron distribution as a broken power-law function of the electron Lorentz factor in the jet ($\gamma_{e,\text{jet}}$) is taken as

$$\frac{dN_{e,\text{jet}}}{d\gamma_{e,\text{jet}}} \propto \begin{cases} \gamma_{e,\text{jet}}^{-2} & \gamma_{m,\text{jet}} \leq \gamma_{e,\text{jet}} \leq \gamma_{b,\text{jet}} \\ \gamma_{e,\text{jet}}^{-p_{\text{jet}}-1} & \gamma_{b,\text{jet}} < \gamma_{e,\text{jet}} \leq \gamma_{M,\text{jet}} \end{cases}, \quad (17)$$

where p_{jet} is the spectral index of electrons accelerated through internal shocks, and $\gamma_{m,\text{jet}}$, $\gamma_{b,\text{jet}}$, and $\gamma_{M,\text{jet}}$ are the minimum Lorentz factor, the break Lorentz factor, and the maximum Lorentz factor of the electrons, respectively. We set $p_{\text{jet}} = 2.3$, $\gamma_{m,\text{jet}} = 5 \times 10^3$, $\gamma_{b,\text{jet}} = 1 \times 10^4$, and $\gamma_{M,\text{jet}} = 2 \times 10^5$. Assuming a zero viewing angle to the jet core axis, we calculate the spectral energy distributions (SEDs) of the emission from the MJC region. The results are shown in Figure 3(a). One can find that the SSC emission component (SSC_{cn}-component) dominates the whole SEDs. More interestingly, the Syn radiation component (Syn_{cn}-component) makes a comparable contribution at the low-frequency end ($\nu < 10^{14}$ Hz). The gamma-ray flux at $\nu > 10^{19}$ Hz is sensitive to $\beta_{\text{cn},0}$.

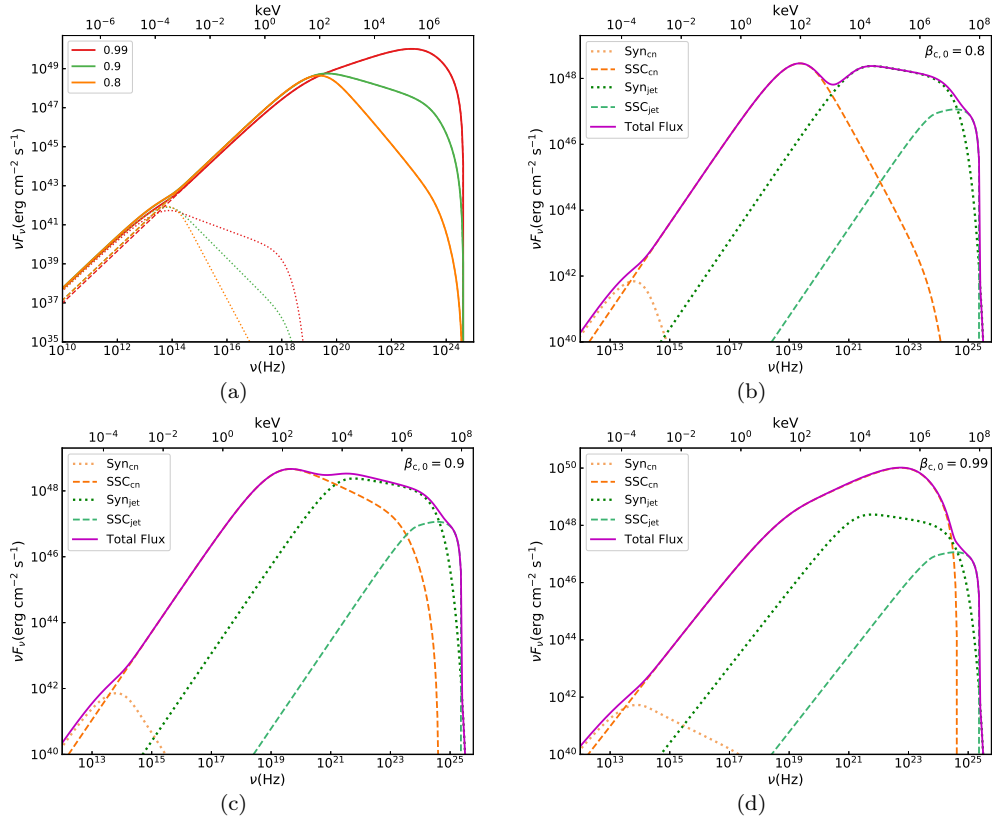


Figure 3. Panel (a)–The SEDs of the shear-accelerated electrons, with the electron distribution corresponding to Figure 2. Panels (b, c, d)– The synthetic SEDs of emissions from the MJC region and the jet core.

The panels b, c, and d of Figure 3 illustrate the radiation SEDs of the jet core and the MJC region with different $\beta_{\text{cn},0}$ values. For a sub-relativistic MJC region ($\beta_{\text{cn},0} = 0.8$ and $\beta_{\text{cn},0} = 0.9$), the SED shape as a semi-Band function in the keV–MeV band, as usually observed with BTASE (Preece et al. 2000). Due to the contribution of the SSC_{cn}-component, the spectral index in the low-energy band is harder than the prediction of the synchrotron emission model. One can find that the predicted SED in the keV–MeV–GeV band exhibits either a Band-cut function or a saddle

shape. Similar SEDs are indeed found in some GRBs observed with the GBM and LAT. In addition, an X-ray excess over the Band-Cut function around 10^{18-19} Hz (several to tens of keV) is found, analogous to the excess observed with the BATSE in the 7–20 keV band (Preece et al. 2000) and with the Swift in the 2–10 keV band (Peng et al. 2014). This excess is attributed to the peak of the SSC_{cn} -component. Thirdly, the Syn_{cn} -component contributes an Inferred-optical flash that may be called as the prompt IR-optical emission. The peak frequency of this flash depends on the magnetic field strength in the MJC region and the initially injected energy of electrons. For the case of a middle-relativistic MJC region ($\beta_{\text{cn},0} = 0.99$) as shown in the panel(d) of Figure 3, the emission originating from the MJC region may dominate the overall SED across a broad range, extending from the optical to the sub-TeV energy bands. The SED in the keV–GeV band still shows up as the shape of the Band function. The sub-TeV emission is attributed to the SSC_{jet} -component.

3. CASE STUDY

The spectral characteristics predicted by our model can potentially accommodate the diversity of the prompt gamma-ray spectra observed with telescopes across different energy bands. In this section, we apply our model to three GRBs (GRBs 090926A, 131108A, and 160509A) whose spectra exhibit a Band-cut or saddle shape. We download the GBM and LAT data of the three GRBs from the public science support center on the official *Fermi* Web site¹. The GBM comprises 12 sodium iodide (NaI) detectors covering an energy range from 8 keV to 1 MeV, and two bismuth germanate (BGO) scintillation detectors sensitive to higher energies between 150 keV and 40 MeV. We select the brightest NaI and BGO detectors. The LAT is a pair conversion telescope with energy coverage ranging from below 20 MeV to over 300 GeV. Data reduction is performed using the *Fermitools-v2.2.0* package and the *P8_TRANSIENT020E* response function. We extract the time-integrated spectra of these GRBs with the GBM and LAT data and fit the data with our model. The observed spectra and our fits are shown in Figure 4. The derived model parameters are listed in Table 1. We describe the results below.

- GRB 090926A: It is a bright, long burst at redshift of $z = 2.1062$ (Malesani et al. 2009). Its T_{90} duration measured with GBM is approximately 21 s (Bissaldi et al. 2009). The derived time-integrated spectrum is accumulated from T_0 to $T_0 + 21.6$ s. It clearly shows a saddle shape. The initial Lorentz factor of its jet core is $\Gamma_{\text{jet}} \sim 600$ (Ackermann et al. 2011). The observed spectrum can be well represented by our model. The bright peak at several hundred of keV is attributed to the SSC_{cn} -component and the broad hump in 10 MeV–10 GeV is dominated by the Syn_{jet} -component. Compared with the jet core, the cocoon is sub-relativistic ($\beta_{\text{cn},0} = 0.83$ vs. $\Gamma_{\text{jet}} = 611$) and low magnetization ($B_{\text{cn}} = 54$ vs. $B_{\text{jet}} = 1 \times 10^6$ G).
- GRB 131108A: It is also a bright burst at $z \sim 2.40$ (Ajello et al. 2019). Its initial Lorentz factor of the jet core is set as $\Gamma_{\text{jet}} \sim 500$ (Ghirlanda et al. 2018). Its SED illustrates a typical Band-Cut function. Our model can well fit the spectrum. Similar to that of GRB 090926A, the SED of GRB 131108A in the keV–MeV band is contributed by the SSC_{cn} -component, and the broad bump at the MeV–GeV band is dominated by the Syn_{jet} -component. The derived model parameters are also similar to those of GRB 090926A.
- GRB 160509A: It is a bright GRB at $z \approx 1.17$ (Tanvir et al. 2016). The prompt emission light curve can be segmented into three distinct phases: a soft “precursor” peak ($T_0 - 5.0$ s $\sim T_0 + 5.0$ s), a bright main episode ($T_0 + 5.5$ s $\sim T_0 + 37$ s), and a subsequent weak emission episode ($T_0 + 300$ s $\sim T_0 + 400$ s) (Vianello et al. 2018). We focus on the radiation characteristics during the primary emission episode that spans from T_0 to $T_0 + 38$ s. The initial Lorentz factor of the jet is set as $\Gamma_{\text{jet}} \sim 300$ (Laskar et al. 2016). Its SED closely resembles the SED of GRB 131108A at $E < 30$ MeV, but has a power-law spectrum in the range from 30–300 MeV range. This power-law decaying segment even extends beyond 1 GeV. We fit the SED with our model and find that the sum of the SSC_{cn} - and the Syn_{jet} -components can well represent the observed SED. The SSC_{cn} -component almost dominates the observed in the keV–MeV–GeV band. The Syn_{jet} -component peaks around 10 MeV, with a peak flux being comparable to the SSC_{cn} -component. The SSC_{cn} -component peaks at ~ 300 keV and decays as a power-law up to 3 GeV. The emission above ~ 0.1 GeV is attributed to the high-energy tail of the SSC_{cn} -component. The B_{cn} of GRB 160509A is 5 \sim 8 times larger than that of GRB 090926A and GRB 131108A. The gamma-ray emission of GRB 160509A in the energy band beyond 100 MeV is attributed to the emission from the

¹ <http://fermi.gsfc.nasa.gov/ssc/data/>

SSC process in the MJC region. We examine the optical depth of the gamma-rays for $\gamma\gamma$ annihilation ($\tau_{\gamma\gamma,\text{cn}}$) in the MJC region of GRB 160509A. The result is shown in Figure 5. It is shown that $\tau_{\gamma\gamma,\text{cn}} < 1$ at < 6 GeV, but it is larger than 1 beyond this energy range. The detection of gamma-rays at $E \sim 3$ GeV in GRB 160509A agrees with the transparency condition.

Table 1. Model parameters derived from our fits to the observed SEDs.

Name	$\beta_{\text{cn},0}$	B_{cn}	$\gamma_{e,\text{inject}}(\Gamma_{\text{jet}})$	B_{jet}	p_{jet}	$\gamma_{m,\text{jet}}$	$\gamma_{b,\text{jet}}$	$\gamma_{M,\text{jet}}$
GRB 090926A	0.830	54	6.11×10^2	1×10^6	2.4	6.5×10^3	9.8×10^3	2×10^5
GRB 131108A	0.895	80	5.02×10^2	1×10^6	2.35	5×10^3	7×10^3	1.3×10^5
GRB 160509A	0.906	450	3.31×10^2	3×10^6	2.1	5×10^3	1.3×10^4	2.5×10^4

4. SUMMARY AND DISCUSSION

Assuming that the GRB jet is structured, we propose that the observed GRB spectrum in the keV–GeV band is attributed to emission from the electrons accelerated via internal shocks in the relativistic jet core and the electrons accelerated through the shear acceleration mechanism in the sub-relativistic MJC region. Taking $\gamma_{e,\text{inject}} = 300$, $B_{\text{cn}} = 100$ G, we show that the SSC process governs the cooling of electrons in the MJC region. The SSC_{cn} emission flux below 10^{19} Hz is almost independent of $\beta_{\text{cn},0}$ but it is sensitive to $\beta_{\text{cn},0}$ at $\nu > 10^{19}$ Hz. Combining both the emission from the jet core and the MJC region, the overall SED in the keV–MeV–GeV band shape as a Band function or a Band-cut function with an X-ray excess if $\beta_{\text{cn},0} \lesssim 0.9$, $B_{\text{cn}} \sim 10^2$ G, $\theta_{\text{cn}} = 0.7$ rad, $\Gamma_{\text{jet}} \sim 300$, $B_{\text{jet}} \sim 10^6$ G, and $\theta_{\text{jet}} = 0.07$ rad. We apply our model to explain the prompt gamma-ray spectra of bright GRBs 090926A, 131108A, and 160509A whose spectra distinctly show two components or a Band-cut function shape. We show that these spectra can be effectively explained with our model.

In this paper, we employ the exponential-decay function to represent the radial velocity profile. Nevertheless, the actual velocity profile may be described as other characteristic functions. We additionally consider a scenario where the velocity profile follows a power-law function and compare the corresponding electron distribution with the exponential-decay case. Figure 6 presents the comparison results using the same parameter set outlined above, with the initial velocity of $\beta_{\text{cn},0} = 0.9$. The results indicate that the structural morphology of shear-accelerated electron distributions persists across different profiles, as described in Eq. 13 and Eq. 14. Variations in the derivative of the velocity profile function affect the efficiency of the shear acceleration process, resulting in differences in the electron distribution. Nonetheless, the primary conclusions of this article remain unaffected.

An X-ray excess over the Band function in the several keV bands has been detected in some GRBs observed with CGRO/BATSE. Preece et al. (1996) analyzed time-averaged spectra from 86 bright GRBs observed during the first five years of BATSE and found that 12 bursts exhibit an excess of low-energy emission in the 5–20 keV range, with a significance exceeding 5σ . A similar signature is also observed with the Ginga observation at energies as low as 2 keV (Strohmayer et al. 1998). It is uncertain whether the X-ray excess is the tip of an ice-burger of the photosphere emission of the “hot” fireball. Inspecting the SEDs shown in Figure 3, one can observe that the sum of the SSC_{cn}-component and the Syn_{jet}-component produce a bump-like feature, which can mimic as an X-ray excess over the fitting curve with the Band function.

¹ This work is supported by the National Natural Science Foundation of China (Grant Nos. 12203015, 12133003). This
² work is also supported by the Guangxi Talent Program (“Highland of Innovation Talents”), and the startup financial
³ support program of Guizhou Normal University (grant No. GZNU2023)].

REFERENCES

- Abbott, B. P., Abbott, R., Abbott, T. D., et al. 2017a, PhRvL, 119, 161101, doi: [10.1103/PhysRevLett.119.161101](https://doi.org/10.1103/PhysRevLett.119.161101)
- , 2017b, ApJL, 848, L13, doi: [10.3847/2041-8213/aa920c](https://doi.org/10.3847/2041-8213/aa920c)
- Ackermann, M., Ajello, M., Asano, K., et al. 2011, ApJ, 729, 114, doi: [10.1088/0004-637X/729/2/114](https://doi.org/10.1088/0004-637X/729/2/114)

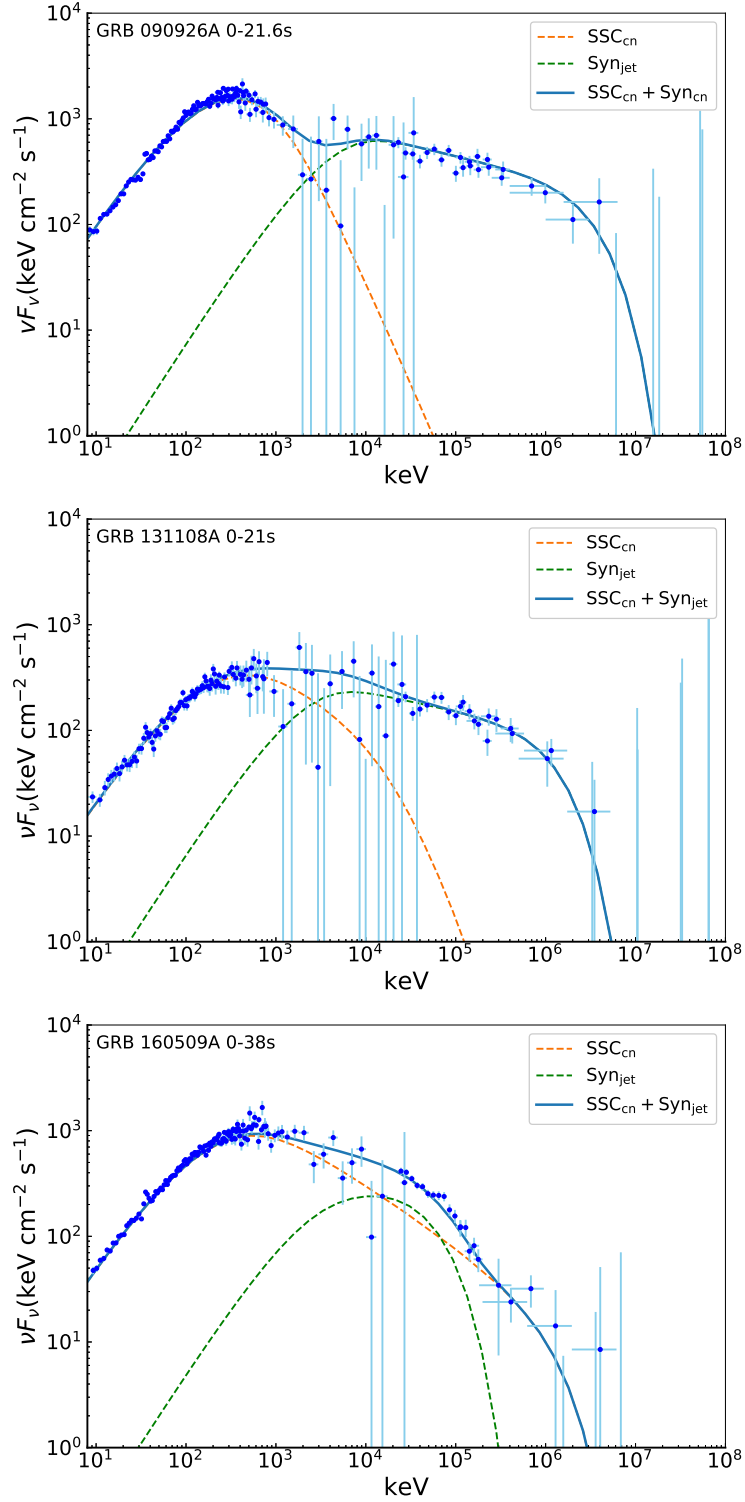


Figure 4. Time-integrated spectra of GRBs 090926A, 131108A, and 160509A, along with theoretical fits by our model (solid lines). The emission components of the MJC and the jet core regions are marked with dashed lines.

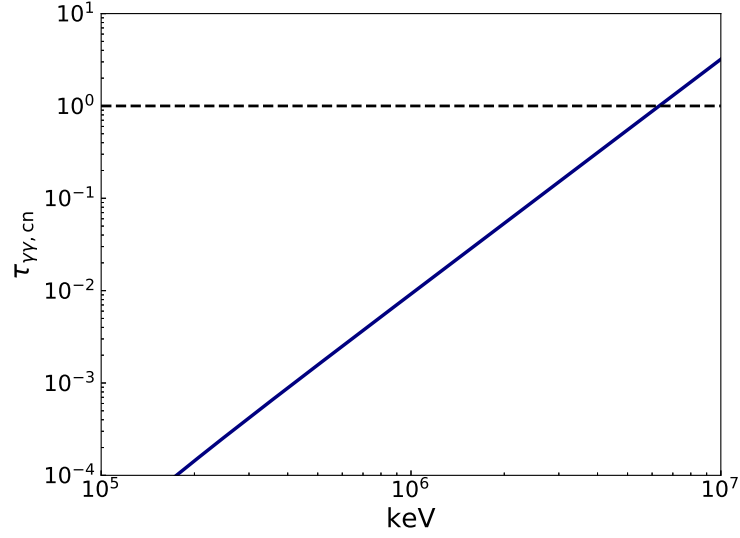


Figure 5. The optical depth for $\gamma\gamma$ annihilation of gamma-ray photons in the MJC region of GRB 160509A as a function of photon energy.

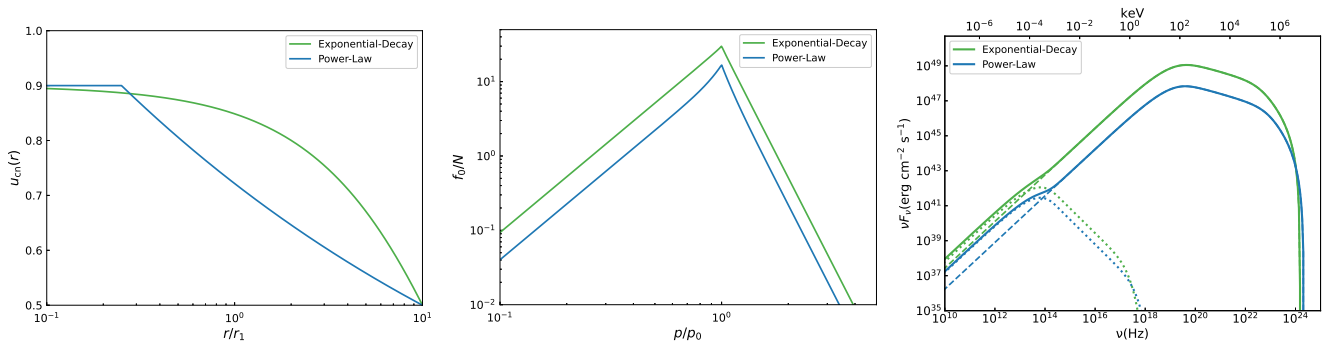


Figure 6. Left panel– Velocity profiles of the MJC region as exponential-decay and power-law functions of radius, with the initial velocity of $\beta_{\text{cn},0} = 0.9$. Right panel– Distributions of shear-accelerated electrons corresponding to the velocity profiles in the left panel.

- . 2013, *ApJS*, 209, 11, doi: [10.1088/0067-0049/209/1/11](https://doi.org/10.1088/0067-0049/209/1/11)
- Ajello, M., Arimoto, M., Asano, K., et al. 2019, *ApJL*, 886, L33, doi: [10.3847/2041-8213/ab564f](https://doi.org/10.3847/2041-8213/ab564f)
- Aloy, M. A., Müller, E., Ibáñez, J. M., Martí, J. M., & MacFadyen, A. 2000, *ApJL*, 531, L119, doi: [10.1086/312537](https://doi.org/10.1086/312537)
- Alves, E. P., Grismayer, T., Fonseca, R. A., & Silva, L. O. 2014, *New Journal of Physics*, 16, 035007, doi: [10.1088/1367-2630/16/3/035007](https://doi.org/10.1088/1367-2630/16/3/035007)
- Alves, E. P., Grismayer, T., Martins, S. F., et al. 2012, *ApJL*, 746, L14, doi: [10.1088/2041-8205/746/2/L14](https://doi.org/10.1088/2041-8205/746/2/L14)
- Band, D., Matteson, J., Ford, L., et al. 1993, *ApJ*, 413, 281, doi: [10.1086/172995](https://doi.org/10.1086/172995)
- Berezhko, E. G., & Krymskii, G. F. 1981, *Soviet Astronomy Letters*, 7, 352
- Biehl, D., Heinze, J., & Winter, W. 2018, *MNRAS*, 476, 1191, doi: [10.1093/mnras/sty285](https://doi.org/10.1093/mnras/sty285)
- Biskamp, D. 2003, *Magnetohydrodynamic Turbulence*
- Bissaldi, E., Briggs, M. S., Piron, F., Takahashi, H., & Uehara, T. 2009, *GRB Coordinates Network*, 9972, 1
- Bromberg, O., Nakar, E., Piran, T., & Sari, R. 2011, *ApJ*, 740, 100, doi: [10.1088/0004-637X/740/2/100](https://doi.org/10.1088/0004-637X/740/2/100)
- Bustamante, M., Heinze, J., Murase, K., & Winter, W. 2017, *ApJ*, 837, 33, doi: [10.3847/1538-4357/837/1/33](https://doi.org/10.3847/1538-4357/837/1/33)
- Daigne, F., & Mochkovitch, R. 1998, *MNRAS*, 296, 275, doi: [10.1046/j.1365-8711.1998.01305.x](https://doi.org/10.1046/j.1365-8711.1998.01305.x)
- Ellison, D. C., Jones, F. C., & Reynolds, S. P. 1990, *ApJ*, 360, 702, doi: [10.1086/169156](https://doi.org/10.1086/169156)
- Frajia, N., De Colle, F., Veres, P., et al. 2019, *ApJ*, 871, 123, doi: [10.3847/1538-4357/aaf564](https://doi.org/10.3847/1538-4357/aaf564)
- Ghirlanda, G., Nappo, F., Ghisellini, G., et al. 2018, *A&A*, 609, A112, doi: [10.1051/0004-6361/201731598](https://doi.org/10.1051/0004-6361/201731598)
- Gill, R., & Granot, J. 2023, *MNRAS*, 524, L78, doi: [10.1093/mnras/slad075](https://doi.org/10.1093/mnras/slad075)
- Goodman, J. 1986, *ApJL*, 308, L47, doi: [10.1086/184741](https://doi.org/10.1086/184741)
- Gottlieb, O., & Globus, N. 2021, *ApJL*, 915, L4, doi: [10.3847/2041-8213/ac05c5](https://doi.org/10.3847/2041-8213/ac05c5)
- Gottlieb, O., Nakar, E., Piran, T., & Hotokezaka, K. 2018, *MNRAS*, 479, 588, doi: [10.1093/mnras/sty1462](https://doi.org/10.1093/mnras/sty1462)
- Kaneko, Y., Preece, R. D., Briggs, M. S., et al. 2006, *ApJS*, 166, 298, doi: [10.1086/505911](https://doi.org/10.1086/505911)
- Keshet, U., & Waxman, E. 2005, *PhRvL*, 94, 111102, doi: [10.1103/PhysRevLett.94.111102](https://doi.org/10.1103/PhysRevLett.94.111102)
- Kolmogorov, A. 1941, *Akademiia Nauk SSSR Doklady*, 30, 301
- Kumar, P., & Zhang, B. 2015, *PhR*, 561, 1, doi: [10.1016/j.physrep.2014.09.008](https://doi.org/10.1016/j.physrep.2014.09.008)
- Laskar, T., Alexander, K. D., Berger, E., et al. 2016, *ApJ*, 833, 88, doi: [10.3847/1538-4357/833/1/88](https://doi.org/10.3847/1538-4357/833/1/88)
- Lazzati, D., & Begelman, M. C. 2005, *ApJ*, 629, 903, doi: [10.1086/430877](https://doi.org/10.1086/430877)
- Lazzati, D., & Perna, R. 2019, *ApJ*, 881, 89, doi: [10.3847/1538-4357/ab2e06](https://doi.org/10.3847/1538-4357/ab2e06)
- Liang, E., Fu, W., & Böttcher, M. 2017, *ApJ*, 847, 90, doi: [10.3847/1538-4357/aa8772](https://doi.org/10.3847/1538-4357/aa8772)
- Liu, R.-Y., Rieger, F. M., & Aharonian, F. A. 2017, *ApJ*, 842, 39, doi: [10.3847/1538-4357/aa7410](https://doi.org/10.3847/1538-4357/aa7410)
- Lyutikov, M., & Blandford, R. 2003, *arXiv e-prints, astro*, doi: [10.48550/arXiv.astro-ph/0312347](https://doi.org/10.48550/arXiv.astro-ph/0312347)
- Malesani, D., Goldoni, P., Fynbo, J. P. U., et al. 2009, *GRB Coordinates Network*, 9942, 1
- Matsumoto, J., & Masada, Y. 2019, *MNRAS*, 490, 4271, doi: [10.1093/mnras/stz2821](https://doi.org/10.1093/mnras/stz2821)
- Mészáros, P. 2002, *ARA&A*, 40, 137, doi: [10.1146/annurev.astro.40.060401.093821](https://doi.org/10.1146/annurev.astro.40.060401.093821)
- Mészáros, P., & Rees, M. J. 2000, *ApJ*, 530, 292, doi: [10.1086/308371](https://doi.org/10.1086/308371)
- Mizuta, A., & Ioka, K. 2013, *ApJ*, 777, 162, doi: [10.1088/0004-637X/777/2/162](https://doi.org/10.1088/0004-637X/777/2/162)
- Mizuta, A., Kino, M., & Nagakura, H. 2010, *ApJL*, 709, L83, doi: [10.1088/2041-8205/709/1/L83](https://doi.org/10.1088/2041-8205/709/1/L83)
- Mooley, K. P., Deller, A. T., Gottlieb, O., et al. 2018, *Nature*, 561, 355, doi: [10.1038/s41586-018-0486-3](https://doi.org/10.1038/s41586-018-0486-3)
- Morsony, B. J., Lazzati, D., & Begelman, M. C. 2007, *ApJ*, 665, 569, doi: [10.1086/519483](https://doi.org/10.1086/519483)
- Murase, K., Asano, K., Terasawa, T., & Mészáros, P. 2012, *ApJ*, 746, 164, doi: [10.1088/0004-637X/746/2/164](https://doi.org/10.1088/0004-637X/746/2/164)
- Nakar, E., Ando, S., & Sari, R. 2009, *ApJ*, 703, 675, doi: [10.1088/0004-637X/703/1/675](https://doi.org/10.1088/0004-637X/703/1/675)
- Nakar, E., & Piran, T. 2017, *ApJ*, 834, 28, doi: [10.3847/1538-4357/834/1/28](https://doi.org/10.3847/1538-4357/834/1/28)
- Narayan, R., Paczynski, B., & Piran, T. 1992, *ApJL*, 395, L83, doi: [10.1086/186493](https://doi.org/10.1086/186493)
- O'Connor, B., Troja, E., Ryan, G., et al. 2023, *Science Advances*, 9, eadi1405, doi: [10.1126/sciadv.adi1405](https://doi.org/10.1126/sciadv.adi1405)
- Paczynski, B. 1986, *ApJL*, 308, L43, doi: [10.1086/184740](https://doi.org/10.1086/184740)
- Pe'er, A. 2015, *Advances in Astronomy*, 2015, 907321, doi: [10.1155/2015/907321](https://doi.org/10.1155/2015/907321)
- Pe'er, A., Mészáros, P., & Rees, M. J. 2006, *ApJ*, 652, 482, doi: [10.1086/507595](https://doi.org/10.1086/507595)
- Peng, F.-K., Liang, E.-W., Wang, X.-Y., et al. 2014, *ApJ*, 795, 155, doi: [10.1088/0004-637X/795/2/155](https://doi.org/10.1088/0004-637X/795/2/155)
- Pilla, R. P., & Loeb, A. 1998, *ApJL*, 494, L167, doi: [10.1086/311193](https://doi.org/10.1086/311193)
- Piran, T. 2004, *Reviews of Modern Physics*, 76, 1143, doi: [10.1103/RevModPhys.76.1143](https://doi.org/10.1103/RevModPhys.76.1143)
- Poolakkil, S., Preece, R., Fletcher, C., et al. 2021, *ApJ*, 913, 60, doi: [10.3847/1538-4357/abf24d](https://doi.org/10.3847/1538-4357/abf24d)

- Preece, R. D., Briggs, M. S., Mallozzi, R. S., et al. 2000, *ApJS*, 126, 19, doi: [10.1086/313289](https://doi.org/10.1086/313289)
- Preece, R. D., Briggs, M. S., Pendleton, G. N., et al. 1996, *ApJ*, 473, 310, doi: [10.1086/178146](https://doi.org/10.1086/178146)
- Ramirez-Ruiz, E., Celotti, A., & Rees, M. J. 2002, *MNRAS*, 337, 1349, doi: [10.1046/j.1365-8711.2002.05995.x](https://doi.org/10.1046/j.1365-8711.2002.05995.x)
- Rees, M. J., & Meszaros, P. 1994, *ApJL*, 430, L93, doi: [10.1086/187446](https://doi.org/10.1086/187446)
- Ren, J., Wang, Y., & Dai, Z.-G. 2024, *ApJ*, 962, 115, doi: [10.3847/1538-4357/ad1bcd](https://doi.org/10.3847/1538-4357/ad1bcd)
- Rieger, F. M., & Duffy, P. 2004, *ApJ*, 617, 155, doi: [10.1086/425167](https://doi.org/10.1086/425167)
- . 2005, *ApJL*, 632, L21, doi: [10.1086/497634](https://doi.org/10.1086/497634)
- Rieger, F. M., & Mannheim, K. 2002, *A&A*, 396, 833, doi: [10.1051/0004-6361:20021457](https://doi.org/10.1051/0004-6361:20021457)
- Sato, Y., Murase, K., Ohira, Y., & Yamazaki, R. 2023, *MNRAS*, 522, L56, doi: [10.1093/mnrasl/slad038](https://doi.org/10.1093/mnrasl/slad038)
- Skilling, J. 1975, *MNRAS*, 172, 557, doi: [10.1093/mnras/172.3.557](https://doi.org/10.1093/mnras/172.3.557)
- Spruit, H. C., Daigne, F., & Drenkhahn, G. 2001, *A&A*, 369, 694, doi: [10.1051/0004-6361:20010131](https://doi.org/10.1051/0004-6361:20010131)
- Strohmayer, T. E., Fenimore, E. E., Murakami, T., & Yoshida, A. 1998, *ApJ*, 500, 873, doi: [10.1086/305735](https://doi.org/10.1086/305735)
- Tang, Q.-W., Wang, X.-Y., & Liu, R.-Y. 2017, *ApJ*, 844, 56, doi: [10.3847/1538-4357/aa7a58](https://doi.org/10.3847/1538-4357/aa7a58)
- Tanvir, N. R., Levan, A. J., Cenko, S. B., et al. 2016, *GRB Coordinates Network*, 19419, 1
- Tchekhovskoy, A., McKinney, J. C., & Narayan, R. 2008, *MNRAS*, 388, 551, doi: [10.1111/j.1365-2966.2008.13425.x](https://doi.org/10.1111/j.1365-2966.2008.13425.x)
- Vianello, G., Gill, R., Granot, J., et al. 2018, *ApJ*, 864, 163, doi: [10.3847/1538-4357/aad6ea](https://doi.org/10.3847/1538-4357/aad6ea)
- Webb, G. M. 1989, *ApJ*, 340, 1112, doi: [10.1086/167462](https://doi.org/10.1086/167462)
- Webb, G. M., Barghouty, A. F., Hu, Q., & le Roux, J. A. 2018, *ApJ*, 855, 31, doi: [10.3847/1538-4357/aaae6c](https://doi.org/10.3847/1538-4357/aaae6c)
- Woosley, S. E. 1993, *ApJ*, 405, 273, doi: [10.1086/172359](https://doi.org/10.1086/172359)
- Yassine, M., Piron, F., Mochkovitch, R., & Daigne, F. 2017, *A&A*, 606, A93, doi: [10.1051/0004-6361/201630353](https://doi.org/10.1051/0004-6361/201630353)
- Zank, G. P., Li, G., Florinski, V., et al. 2004, *Journal of Geophysical Research (Space Physics)*, 109, A04107, doi: [10.1029/2003JA010301](https://doi.org/10.1029/2003JA010301)
- Zhang, B., & Yan, H. 2011, *ApJ*, 726, 90, doi: [10.1088/0004-637X/726/2/90](https://doi.org/10.1088/0004-637X/726/2/90)
- Zhang, B.-B., Zhang, B., Liang, E.-W., et al. 2011, *ApJ*, 730, 141, doi: [10.1088/0004-637X/730/2/141](https://doi.org/10.1088/0004-637X/730/2/141)
- Zhang, W., Woosley, S. E., & MacFadyen, A. I. 2003, *ApJ*, 586, 356, doi: [10.1086/367609](https://doi.org/10.1086/367609)
- Zrake, J., & MacFadyen, A. I. 2012, *ApJ*, 744, 32, doi: [10.1088/0004-637X/744/1/32](https://doi.org/10.1088/0004-637X/744/1/32)